Nitrate Radical Quantum Yield from Peroxyacetyl Nitrate Photolysis

Bradley A. Flowers,† Mark E. Angerhofer, William R. Simpson,* Tomoki Nakayama,‡ and Yutaka Matsumi‡

Department of Chemistry and Geophysical Institute, University of Alaska, Fairbanks, Fairbanks, Alaska 99775-6160

Received: October 1, 2004; In Final Form: January 7, 2005

Peroxyacetyl nitrate (PAN, $CH_3C(O)OONO_2$) is a ubiquitous pollutant that is primarily destroyed by either thermal or photochemical mechanisms. We have investigated the photochemical destruction of PAN using a combination of laser pulsed photolysis and cavity ring-down spectroscopic detection of the NO_3 photoproduct. We find that the nitrate radical quantum yield from the 289 nm photolysis of PAN is $\Phi_{NO_3}^{PAN} = 0.31 \pm 0.08$ ($\pm 2\sigma$). The quantum yield is determined relative to that of dinitrogen pentoxide, which is assumed to be unity, under identical experimental conditions. The instrument design and experimental procedure are discussed as well as auxiliary experiments performed to further characterize the performance of the optical cavity and photolysis system.

Introduction

Polluted environments contain NO_2 and partially oxidized hydrocarbons that react to form peroxyacetyl nitrate (PAN, $CH_3C(O)OONO_2$). PAN remains stable enough at low temperature to transport NO_2 to remote regions of the globe.[1,2] PAN is only slowly removed by OH radical oxidation and dry and wet deposition.[1,3] Due to these properties, PAN contributes significantly to the long-range transport of NO_2. The thermal stability of PAN is primarily reponsible for its accumulation in the arctic during winter. Thermolysis via

$$CH_3C(O)O_2NO_2 + M \rightleftharpoons CH_3C(O)O_2 + NO_2 + M \quad (1)$$

has been studied extensively as the predominant ground-level PAN loss process.[1,4] Further experiments have indicated that the thermal decomposition of PAN proceeds dominantly via (1) despite near isoenergy of the O−O and O−N single bonds in PAN.[4,5] Process (1) is strongly temperature dependent,[6] leading to a PAN lifetime with respect to thermal decomposition of 1 month at 255 K. Recombination via (−1) extends the effective thermal lifetime. Field measurements indicate that PAN is the predominant active nitrogen species (NO_y) during the winter to spring transition at high latitudes.[7] Typical arctic temperatures are sufficiently low enough to preclude thermal decomposition as the sole viable PAN loss mechanism throughout the winter and spring at ground level and at high altitude.[7,8]

The second loss process for atmospheric PAN is photolysis. Many possible photoproducts may be formed by UV photolysis as reviewed by Mazely, Friedl, and Sander.[9,10] Two major decomposition channels dominate for UV photolysis,

$$CH_3C(O)O_2NO_2 + h\nu \rightarrow CH_3C(O)O_2 + NO_2 \quad (2)$$

$$CH_3C(O)O_2NO_2 + h\nu \rightarrow CH_3C(O)O + NO_3. \quad (3)$$

The absorption cross section for PAN has been measured.[3,11] The work of Talukdar et al. demonstrates a 40% decrease in σ_{PAN} at 320 nm between 298 and 250 K.[3] Due to the instability of the acetoxy radical produced in (3), photolysis in this channel leads to irreversible loss of PAN. Subsequently, NO_3 is photolyzed to NO_2 or NO by visible light; therefore (3) directly converts PAN to NO_x and is an irreversible loss from the PAN reservoir. For PAN photolysis resulting in (2), the photoproducts remain stable and can recombine to re-form PAN, thereby extending the effective lifetime of the PAN reservoir. Thus, the PAN photolysis channels (2) and (3) affect the PAN reservoir very differently.

Laser-induced fluorescence (LIF) detection of NO_2 and NO_3 photoproducts following 248 nm photolysis of PAN measured the quantum yield of NO_2 ($\Phi_{NO_2}^{PAN}$) to be 0.70 ± 0.10[9] and $\Phi_{NO_3}^{PAN}$ to be 0.30 ± 0.10.[10] Recently, the nitrate radical quantum yield from PAN photolysis was investigated again at 248 nm and also at 308 nm detecting NO_3 using laser absorption spectroscopy.[12] In both studies $\Phi_{NO_3}^{PAN}$ was determined relative to Φ_{NO_3} from N_2O_5 photolysis. The 248 nm results of the Harwood et al. study are slightly different from the previously reported results of Mazely et al. $\Phi_{NO_3}^{PAN}$ (248 nm) $= 0.19 \pm 0.04$. Harwood et al. indicate that the previous work of Mazely et al. used an incorrect value for $\Phi_{NO_3}^{N_2O_5}$ at 248 nm and that after correction, the agreement between the studies is acceptable, indicating approximately 20% NO_3 production. Harwood et al. also measured the photolysis quantum yield for NO_3 at 308 nm and found $\Phi_{NO_3}^{PAN}(308\text{ nm}) = 0.41 \pm 0.10$. The results of these studies[9,10,12] suggest that NO_2 and NO_3 (and their respective organic radicals) are the major direct photoproducts of PAN photolysis at or above 248 nm. It also appears that the nitrate radical quantum yield from PAN is wavelength dependent. While the results so far reported[9,10,12] indicate that NO_2 is the dominant direct photoproduct in PAN photolysis, $\Phi_{NO_3}^{PAN}$ cannot be discounted due to the differences in resulting atmospheric chemistry of the two photolysis channels.

In the present work, PAN photolysis was studied at a photolysis wavelength of 289 nm using cavity ring-down absorption spectroscopy (CRDS) to detect nitrate radicals.[13] The

* To whom correspondence should be addressed. E-mail: ffwrs@uaf.edu.
† Permanent Address: Department of Chemistry and Biochemistry, The University of Texas at Austin, Austin, TX 78712.
‡ Present address: Solar-Terresterial Environment Laboratory and Graduate School of Science, Nagoya University, Toyokawa, Japan 442-8507.

10.1021/jp045529n CCC: $30.25
Published on Web 02/26/2005

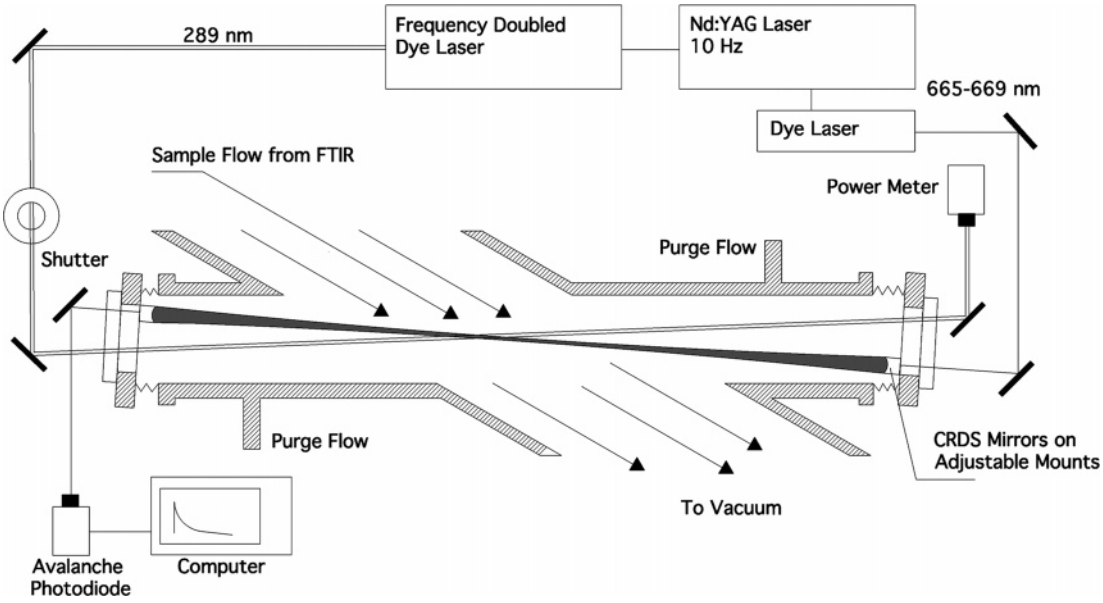

Figure 1. Pulsed CRDS photolysis-flow experimental schematic. Not drawn to scale.

photolysis wavelength was chosen to coincide with the beginning of the solar flux available for atmospheric photochemisty. The description of the instrument and experimental technique is given along with analysis of these results at 289 nm in the following sections.

Experiment

Samples of N_2O_5 and peroxyacetyl nitrate (PAN) are photolyzed, producing NO_3 radicals that are detected by cavity ring-down absorption measurements. The relatively low number density of NO_3 due to weak absorption of PAN at 289 nm is overcome using the high sensitivity of CRDS pulsed photolysis-flow experiments described below. Using CRDS to detect photochemical reaction products has been reported previously by several research groups.[14,15] Figure 1 is a schematic drawing of the experiment. The flow chamber is constructed of a 100 cm long, 7.6 cm outer diameter stainless steel tube with a 50 cm long, 3.8 cm outer diameter set of arms crossing its center at 30 °. A mechanical vacuum pump (Edwards E2M18) is used to evacuate and flow samples in the main chamber. The sample flow rate was sufficient to replace completely the precursor gases every laser shot. Total system pressure is measured by a capacitance manometer (MKS Baratron Type 622) connected via 1.3 cm outer diameter Ultratorr fitting directly atop the center crossing point.

The photolysis windows and cavity mirrors are held to the ends of the crossing volume with 6.9 cm diameter bellow flanges held in adjustable mounts to allow alignment of the ring-down cavity. The ring-down cavity is formed by two high-reflectivity mirrors (Research Electro Optics). The reflectivity of these mirrors is 0.99995 and optimal alignment of the 50 cm long cavity produced empty cavity ring down times of 37 μsec. To produce the CRDS probe beam, 5% of a pulsed Nd:YAG laser beam (Spectra Physics Quanta Ray Lab 150) pumps a dye laser (Dakota Technologies Northern Lights) filled with DCM dye. The dye laser typically produces 1.0 mJ per pulse. The CRDS beam passes through focusing optics and an iris to condition the beam in an attempt to excite primarily low order cavity modes. Selection of low-order cavity modes decreases the noise in the CRDS measurement. To detect the strong ($\tilde{B} \leftarrow \tilde{X}$) electronic absorption band of NO_3 centered at 662 nm, the dye laser is scanned from 655 to 669 nm in 0.5 nm steps. The ring-down signal is detected by an avalanche photodiode detector (Hamamatsu C5460) and read into a computer by use of LabVIEW virtual instruments (National Instruments).

The main beam (95%) from the Nd:YAG laser is directed to a second dye laser (Sirah Cobra Stretch). The 289 nm UV light is produced by frequency doubling the 578 nm output of Rhodamine 6G dye laser using a KDP doubling crystal. The pump and probe beams cross in the center of the flow chamber at a 2.1° angle. In this crossing geometry the CRDS beam ($\leq$1 mm^2) probes the interior of the photolysis beam (3 mm^2). Typical photolysis energies of 1 mJ are used. Maximum output energy of the photolysis laser is 3.3 mJ, and the energy is attenuated by rotatable half-wave plate/polarizer optics[20] placed in the beam path before the photolysis beam entered the flow chamber. With these optics, the photolysis beam could be attenuated between 0 and 3.0 mJ.

Initially, the baseline ring-down time was found to decay due to heating of the CRDS mirrors from the photolysis beam. The CRDS mirrors are coated with Ta_2O_5 layers that absorb in the UV, causing this heating. To decrease the UV heating problem, the chamber windows were replaced with antireflective coated windows that had $\leq$0.05% UV reflection. The decreased reflectivity caused less scattered UV to be present in the chamber and minimized the UV heating effect.[18] To remove residual effects due to UV mirror heating, a rapid background subtraction procedure is used. Both photolysis and the CRDS beams are driven at the 10 Hz repetition of the Nd:YAG laser. Between the main chamber and the UV photolysis laser is a shutter timed to allow five UV pulses through and to block five pulses hereby establishing photolysis on and off states of the experiment. We then observe the change in ring down time between photolysis on and off states to observe photochemistry specifically. The 1 Hz shutter frequency proved fast enough that no heating was observable in the difference between on and off states. By maintaining total pressures of 10 Torr and a flow rate of 0.1 SLPM in the main flow chamber, we were able to completely flush the photoproducts between successive laser shots.[18]

A purge flow of N_2 is used between the main flow and mirrors to minimize contamination of the CRDS mirrors. Because of this purge gas, the mirror-to-mirror length (ℓ = 50 cm) of the ring-down cavity is not completely filled by precursor gases.

Separate experiments using water vapor showed that approximately 15 cm along the cavity axis were filled by flowing precursor gases. In the pump−probe experiments, only the coincident region between the photolysis and CRDS laser beams is sampled. We estimate this crossing length to be ∼7 cm and is entirely within the flowing precursor gas. However, the precise value of this crossing length is not important because the PAN quantum yield is measured relative to a reference molecule, N_2O_5, as described later.

Peroxyacetyl nitrate samples are synthesized by the technique of Gaffney et al.[17] and stored at 220 K. To supply PAN to the photolysis experiment, a flow of N_2 carrier gas is bubbled through PAN sample in tridecane solvent placed in a ethylene glycol/water bath chilled to 269K. The typical number density of PAN is $(3-30) \times 10^{14}$ molecules cm^{-3}. Dinitrogen pentoxide is synthesized in a home-built glass rack using a method similar to Davidson et al..[23] Briefly, N_2O_5 is trapped as a product of the reaction between NO_2 and excess O_3. After several freeze/thaw/react/trap cycles the NO_2 charge introduced to the glass rack is completely oxidized to N_2O_5 and stored at 220 K. The N_2O_5 sample was stored in dry ice/trichloroethylene slush bath during use. Typical concentrations of $(1-5) \times 10^{14}$ molecules cm^{-3} N_2O_5 are supplied for photolysis experiments. The purity of both samples was established by FTIR absorption and used without further purification. Both samples are supplied to the vacuum chamber through PFA Teflon tubing from their respective baths. The loss of either sample to the surface of the tubing and vacuum chamber was tested by switching the flow order to have the FTIR quantification either before or after the sample chamber. This test showed negligible loss of precursor gases.[18]

Precursor concentrations are measured upstream of the photolysis chamber by an FTIR absorption spectrometer (Perkin-Elmer Paragon 1000, 4.0 cm^{-1}resolution). The precursor gases passed through a 17.3 cm length flow cell with CaF_2 windows housed permanently in the FTIR sample chamber. Gas concentrations were determined by fitting the FTIR spectrum over the region 1000−2000 cm^{-1} to a linear combination of spectra of the precursor gas and other possible impurities. A nonlinear Levenberg-Marquart algorithm was used in the fitting (Wavemetrics Igor Pro). In this manner, both the precursor gas concentration and possible impurities were quantified. For PAN quantification, the spectra of PAN, acetyl nitrate, acetic acid, nitric acid, as well as a linear slope and offset were used. All reference spectra were measured on our FTIR spectrometer. For quantification of PAN, the integrated cross sections of Tsalkani and Toupance[16] were used to scale the standard reference spectrum. The maximum percent error on these cross sections is reported to be 2% for the 1163.5 cm^{-1} peak. The cross sections of Gaffney et al.[17] are similar except for the 1740.5 cm^{-1} peak, as described in Tsalkani and Toupance.[16] The reported errors for the cross sections are significantly less than the instrumental precision in the number densities measurement (∼ 10−20%), thus the cross section error is not propagated through the number density calculations. In all cases we find the concentration of selected impurities negligible. Also, no impurity in the PAN sample has an NO_3 photoproduct at the photolysis wavelength. For N_2O_5 quantification, the same method was used, but the reference spectra of N_2O_5, NO_2, H_2O and nitric acid were used in addition to the linear slope and offset. The N_2O_5 reference spectrum was scaled by using the cross section of Wangberg et al. at 1245 cm^{-1}($\sigma_{N_2O_5} = 8.56 \times 10^{-19}$ cm^2 $molecule^{-1}$).[19] The NO_2 reference spectrum quantification was also taken from Wangberg et al. at 1602 cm^{-1}($\sigma_{NO_2} = 4.71 \times 10^{19}$ cm^2 $molecule^{-1}$). No error is given by the report of Wangberg et al., and no error is assumed for these cross sections in this work either. Although HNO_3 contamination was sometimes present in the N_2O_5 samples, the NO_3 quantum yield from HNO_3 photolysis is very low (<0.002),[26] thus nitric acid did not contribute to photolytic NO_3 significantly in these experiments.

When using the N_2O_5 sample, the carrier gas is seeded with $\sim 10^{14}$ molecules cm^{-3} of NO_2. The added NO_2 decreases the thermal NO_3 background in the N_2O_5 sample by forcing the chemical equilibrium $NO_2 + NO_3 \rightleftharpoons N_2O_5$ toward N_2O_5.[19,24] Because the NO_2 is present throughout the photolysis modulation cycle, its absorption is removed by differencing between the absorption measured in photolysis on and off states. A small fraction of the NO_2 is photolyzed to produce NO, which reacts rapidly with NO_3 ($k_{289} = 2.6 \times 10^{-11}$ cm^3 $molecule^{-1}$ s^{-1}) and thus could present a photolytic impurity. However, only $\sim 10^{11}$ molecules cm^{-3} of NO are formed, leading to a lifetime of NO_3 of ∼0.4 s., which is longer than both the ring-down time scale and the flow flushing time scale. Therefore, addition of NO_2 has only the desired effect of suppression of thermal NO_3 background.

In the relative quantum yield experiments, a scan of the detection range was performed during photolysis of N_2O_5, then the photolysis chamber was isolated from the N_2O_5 flow and evacuated. After evacuation, the carrier flow was switched to the PAN sample then that flow was introduced to the photolysis chamber at the same conditions. We then switched back to flowing the N_2O_5 sample to bracket the PAN photolysis measurements. The CRDS detection range was scanned at 4 nm per minute. This scan rate covers the detection range in 4 min, so 4 FTIR scans at 70 s each were taken concurrently to determine the precursor concentration as a function of time during the scan. The concentration of N_2O_5 supplied to the photolysis experiment was controlled by the temperature of the bath. It was found to be straightforward to maintain relatively constant concentrations of N_2O_5 over the course of the experiment. Despite our best efforts, the PAN concentration decreases rapidly over the duration of the experiment. The final concentration of PAN was typically found to be half the concentration at the beginning of the spectral scan. Much of this decay affects the wings of the NO_3 spectrum and is thus not critical for accurate determination of the amount of photolytic NO_3, but we sought a systematic method to remove this precursor concentration decay.

During each experiment, the four determinations of precursor concentration were fitted to an exponential or linear decay function. This decay function was then normalized to unity at the time when the NO_3 product scan was at the 662 nm absorption peak. We then divided each of the four FTIR determinations by the normalized decay function to give a detrended precursor concentration. The average and standard deviations of these detrended precursor concentrations are shown in Table 1. The difference in absorption from the CRDS measurements are also divided by the same normalized precursor decay function, determined by FTIR, resulting in a detrended product absorption spectrum. This product spectrum is then fitted to a literature NO_3 spectrum for quantification of the amount of NO_3 produced in the experiment. The error on the NO_3 measurement comes from the error estimate in the nonlinear least-squares fitting procedure. Photolysis pulse energy was monitored throughout each run to ensure that a constant photolysis energy was maintained for the experiment.

TABLE 1: Number Densities and Quantum Yields for PAN/N_2O_5 Photolysis Experiments at 289 nm

expt no.	$[N_2O_5]^a$	$[PAN]^a$	NO_3 ratio	$\Phi_{NO_3}^{PAN}$
1	1.30 ± 0.10	6.49 ± 0.89	0.14 ± 0.01	0.35 ± 0.06
2	2.37 ± 0.02	27.7 ± 0.3	0.23 ± 0.01	0.24 ± 0.01
3	1.31 ± 0.10	3.37 ± 0.19	0.08 ± 0.01	0.39 ± 0.06
4	0.84 ± 0.02	2.76 ± 0.02	0.08 ± 0.01	0.30 ± 0.04
5	5.43 ± 0.51	5.81 ± 1.50	0.024 ± 0.002	0.28 ± 0.08
6	4.44 ± 0.42	4.28 ± 0.55	0.024 ± 0.001	0.31 ± 0.05

[a] Number densities are reported per 10^{14} molecules cm^{-3}. The uncertainties reported for the number densities are 2σ. The NO_3 ratio error is described in the text.

Results and Discussion

The photolytic NO_3 concentration is determined from the difference of absorption between photolysis on and off states. For both states the measured ring-down time, (τ), is converted to a loss rate per distance, $r = (c\tau)^{-1}$, which is proportional to the optical absorption. The difference in loss rate, Δr, between photolysis on and off values is related to the photolytic change in $[NO_3]$ number density by

$$\Delta r = \frac{1}{c}\left(\frac{1}{\tau_{ON}} - \frac{1}{\tau_{BL}}\right)\frac{\ell}{\ell_s} = \Delta[NO_3]\sigma_{NO_3}. \quad (4)$$

The absorption cross section σ_{NO_3} used in this analysis is taken from the 2003 JPL reference.[26] Many researchers have measured this cross section and have found different values, indicating significant uncertainty in the actual peak cross section of NO_3 absorption, however the actual peak value is unimportant for the present experiment because only relative amount of NO_3 formed between the PAN and N_2O_5 photolysis experiments enters into the final analysis. The cavity length scaling factor (ℓ/ℓ_s) describes the fraction of the total cavity length, ℓ, divided by the length that is filled by absorber, ℓ_s. These values were described in the Experimental Section and are not critical because of the use of a reference molecule. The ring-down time of the photolysis off state is τ_{BL} and the ring-down time for the photolysis on state is τ_{ON}. Typical total NO_3 number densities of $\sim 10^9$ molecules cm^{-3} NO_3 were detected. Previous work on this system has indicated that the detection limit for NO_3 is approximately 2×10^7 molecules cm^{-3}.[18]

Quantitative measurement of the NO_3 quantum yield from PAN photolysis requires that the photolytic NO_3 is detected more rapidly than is lost due to motion away from the photolysis volume or lost by chemical reaction. Therefore, we studied the temporal behavior of the ring-down decay profiles to ensure no loss of NO_3 on the relevant time scale, which is on the order of the ring-down time. Figure 2 shows the ring-down decay profile for N_2O_5 photolysis with NO_3 detection at 662 nm. The filled circles show the baseline decay profile, in the absence of photolysis, while the open circles show the photolytic decay profile. The open circles decay more rapidly due to increased absorbance of the photoinduced NO_3. The flat plateau at early time in both profiles is due to a detector cutoff at 9 V and is ignored in the analysis routine. We intentionally align the system to have some cutoff intensity to remove rapidly decaying high-order mode cavity excitations from the ring-down profile. These higher-order modes would cause nonexponential ring-down decay profiles and cause increased noise in the CRDS measurement. Inspection of both profiles shows nearly exponential decays before the signal decays into noise. The observation of an exponential decay for the photolytic (open) data indicates that the concentration of NO_3 is constant over the decay profile.

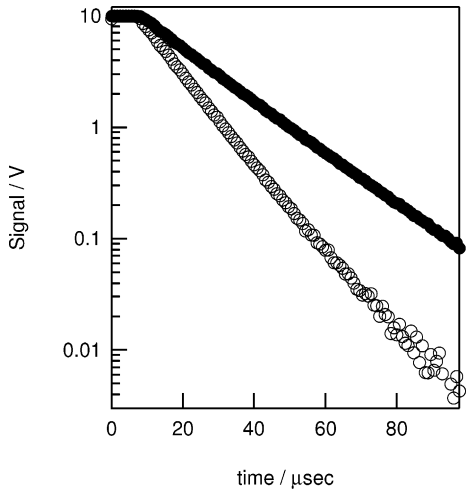

Figure 2. Ring-down signal decay profiles for photolysis off (dark) and photolysis on (empty) states during N_2O_5photolysis.

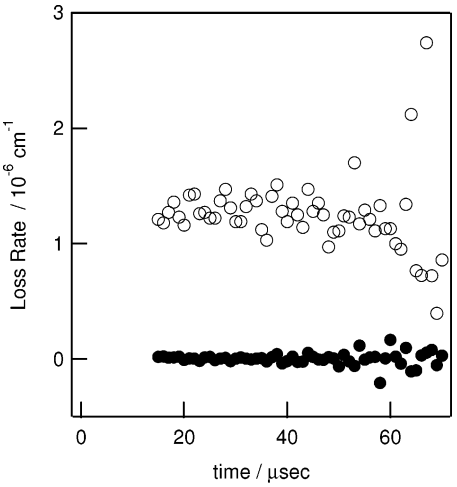

Figure 3. Temporal profile of the cavity loss rate measured in the presence of NO_3 (empty circles) and the empty cavity loss rate (dark circles). Individual data are the result of the photolytic differencing procedure described in the text.

A very careful examination of the ring-down decays shown in Figure 2 shows a slightly nonexponential decay behavior in both photolytic and nonphotolytic signals. To establish that the slight deviation of the ring-down waveforms from exponential behavior is not caused by temporal changes in the photolytic radical number density observation, the temporal profile of the cavity loss rate *r(t)* was determined. Figure 3 shows the calculated instantaneous loss rates (r) for the cavity in the presence of NO_3 (open circles) and absence of sample (dark circles). The change in loss rate with time is calculated as the difference between slopes of the intensity decay during modulated photolysis with and without N_2O_5 present in the cavity. This kinetic analysis was presented in detail in the work of Brown et al.[15] termed SKaR (simultaneous kinetics and ring-down). In our case, however, we are interested in ensuring that there is no NO_3 loss on the time scale of the ring down event. The data points shown Figure 3 are differences between r values for photolysis states via

$$\Delta r = \frac{1}{c}\left[\frac{d(\ln I(t))}{dt}_{ON} - \frac{d(\ln I(t))}{dt}_{OFF}\right] \quad (5)$$

The dark circles in Figure 3 are the difference between loss rates with and without photolysis in the absence of sample. The

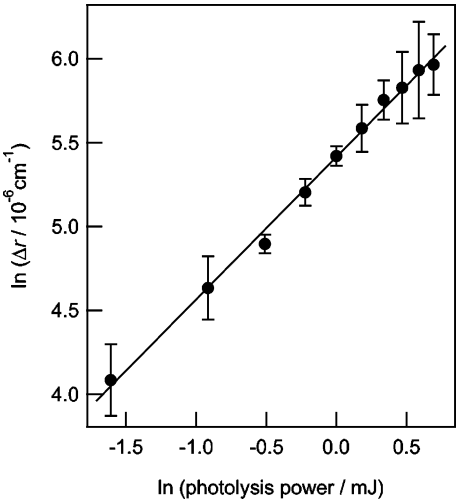

Figure 4. Plot of the natural logarithm of the photolytic difference in optical loss, Δr, vs the natural logarithm of the photolysis power. The photolysis power was varied between 0 and 2.0 mJ to measure the power dependence for N_2O_5 photolysis. The slope of the line is 0.9 ± 0.1, indicating a linear relationship between power and signal for N_2O_5 photolysis up to 2.0 mJ.

zero value indicates that the rapid photolysis modulation removes any effect of mirror heating. The open circles are the difference in loss rates observed during N_2O_5 photolysis. By inspection of the data up to ~40 μs, the loss rate of the cavity in the presence of NO_3 varies by less than 10%. Taken together, the data shown in Figures 2 and 3 show that the photolytic [NO_3] is constant on the time scale of the ring-down event; i.e, the bulk flow rate of sample into the vacuum chamber is not removing NO_3 on the experimental time scale. An additional concern is the possibility of the photolysis event depositing thermal energy in the NO_3 fragments such that the hot fragments fly out of the CRDS probe region while they are being detected. At longer ring down times there would effectively be less NO_3 to detect and the open circles in Figures 2 and 3 would approach the dark circles. Clearly we do not observe this flyout effect. Torabi[27] reported a relaxation time for vibrationally hot NO_3 produced from N_2O_5 photolysis of 7 μs in 50 Torr of He. Our conditions are at lower pressure, 10 Torr, but with a more efficient collisional quencher, nitrogen gas, thus one might expect a similar time scale for collisional quenching. We see no evidence of changes in the concentration of NO_3 early in the ring-down decay profile, thus any affect of this vibrational relaxation is not evident in our experiment. Additionally, the un-analyzed signal saturation in the beginning of the ring-down decay (~10 μs) may preclude observation of effects from this collisional relaxation. Thus, we conclude that cavity ring-down spectroscopy of the NO_3 $\tilde{B} \leftarrow \tilde{X}$ band quantitatively measures the product from these photolysis reactions.

Another requirement for determining a photolysis quantum yield for one species relative to another is that both species must be undergoing one-photon photolysis reactions. In this case, N_2O_5 has a larger absorption cross section at 289 nm than does PAN. Therefore, we sought to ensure that we are observing a one-photon photolysis process for N_2O_5. If linear photochemistry is observed for N_2O_5 photolysis, it will be so for the weaker absorbing PAN photolysis as well. A power dependence study for N_2O_5 photolysis was performed detecting NO_3 at 662 nm using CRDS. By using the polarizer/wave plate optic, the photolysis power used for N_2O_5 photolysis was varied from 0 to 2.0 mJ by 0.2 mJ increments. The results from this study are shown in Figure 4, which plots the natural logarithm of the photolysis power vs the natural logarithm of the NO_3 signal observed. The NO_3 signal observed at each power datum was normalized by the absorbance of N_2O_5 recorded upstream by the FTIR spectrometer. The points in Figure 4 are the result of averaging four measurements at each photolysis power. The slope of the log−log plot is the order of the power dependence, N, and should be 1 for a one-photon process. The slope of the data in Figure 4 indicates that $N = 0.9 \pm 0.1$, therefore we are confident that for photolysis powers used in our experiment we are observing a one-photon process for N_2O_5 and subsequently PAN photolysis up to 2.0 mJ per pulse.

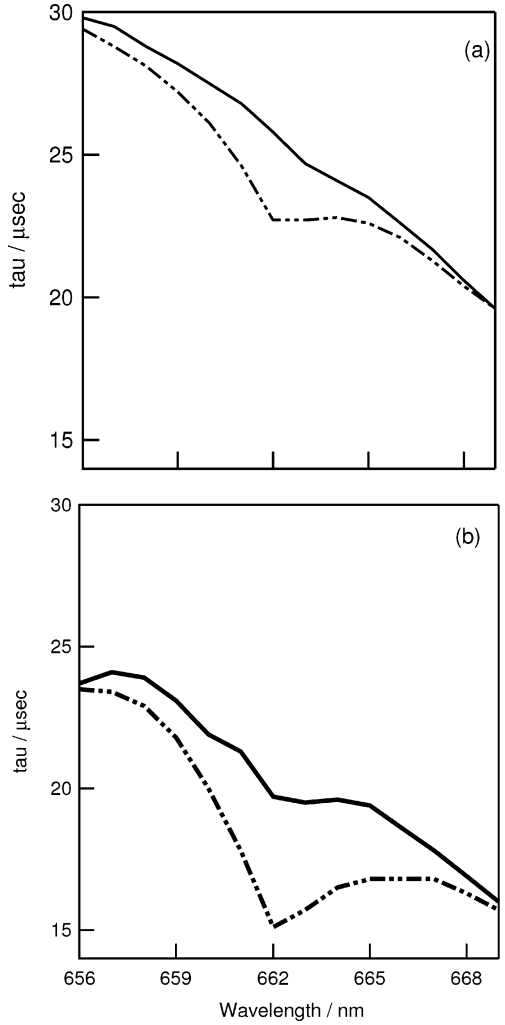

Figure 5. Ring down times τ_{ON} and τ_{BL} recorded for photolysis on (dashed) and off (solid) states during PAN (a) and N_2O_5 (b) photolysis. The general decrease in τ_{BL} is due to the transmission of the CRDS mirrors. The dip in the solid line at 662 nm in part b is the detection of thermal NO_3 from N_2O_5 thermolysis. This background signals are eliminated through the differencing procedure described in the text. To minimize this background in practice the flow of N_2O_5 was seeded with NO_2. This NO_2 shows some small absorption features, most notably at 656 nm.

Raw data from N_2O_5 and PAN photolysis are shown in Figure 5, parts a and b, respectively. The general decrease in τ_{BL} vs wavelength is characteristic of the reflectivity of the mirrors used in the cavity, which decreases at longer wavelengths. In Figure 5b, the additional decrease in τ_{BL} at 662 nm without photolysis is due to absorption of background NO_3 from N_2O_5 thermal decomposition. This spectral feature is further evidenced by the return of τ_{BL} to its wavelength transmission near 665 nm. The thermal NO_3 is removed from the photolytic NO_3 number density by the differencing procedure in (4). The CRDS

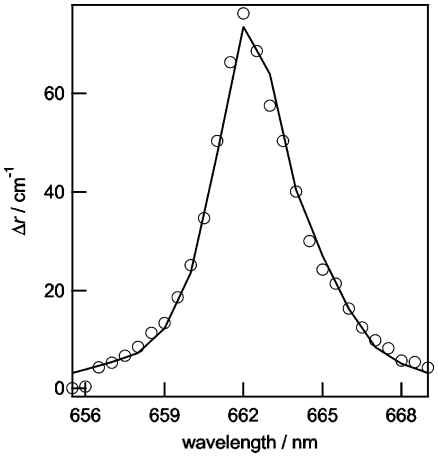

Figure 6. CRDS difference spectra recorded during N_2O_5 photolysis at 289 nm. The open circles are the difference between optical loss (r) observed in the presence and absence of photolysis. The solid line is a reference spectrum of NO_3 taken from the JPL compendium.[26]

laser wavelength scan is compared to a reference spectrum of NO_3 to eliminate the possibility that additional absorbers contribute to the NO_3 absorption measurement.

The nitrate radical quantum yield from PAN relative to N_2O_5 is determined by

$$\Phi_{NO_3}^{PAN} = \Phi_{NO_3}^{N_2O_5} \times \frac{[NO_3]_{PAN}}{[NO_3]_{N_2O_5}} \times \frac{\sigma_{N_2O_5}}{\sigma_{PAN}} \times \frac{\tilde{N}_{N_2O_5}}{\tilde{N}_{PAN}}. \qquad (6)$$

Here σ_x is the UV absorption cross section of either PAN or N_2O_5, $[NO_3]_x$ is the nitrate radical concentration detected from either PAN or N_2O_5 photolysis, and $\tilde{N}_x$ is the precursor concentration of PAN or N_2O_5 measured upstream of the photolysis chamber via FTIR. The NO_3 quantum yield from N_2O_5 at 289 nm is assumed to be unity. The accepted value for $\Phi_{NO_3}^{N_2O_5}$ has been the topic of some discussion, however the available results indicate that at wavelengths longer than 248 nm, $\Phi_{NO_3}^{N_2O_5}$ approaches unity rapidly.[25,26] The 248 nm $\Phi_{NO_3}^{N_2O_5} = 0.8 \pm 0.1$, while at 308 nm, the quantum yield is unity.[25] Simple linear interpolation between these two values indicates a 289 nm $\Phi_{NO_3}^{N_2O_5} = 0.96$, which is within the 248 nm experimental error of unity. Therefore, we assume that the 289 nm $\Phi_{NO_3}^{N_2O_5} = 1.0$ and propagate 10% error for this assumption. Because the photolysis measurements are done under identical experimental conditions for both PAN and the N_2O_5 reference, the crossing volume length from (4) cancels. The precursor detrended photolytic difference spectra for nitrate radical from PAN and N_2O_5 photolysis are fitted to a NO_3 reference spectrum and shown in Figures 6 and 7. The open circles represent the difference between NO_3 absorption in the dark and light states of the experiment. The solid line is a reference spectrum of nitrate radical taken from the JPL reference.[26] Only the relative NO_3 number density is of interest, making the absolute value used for σ_{NO3} unimportant. From the agreement between the difference and reference spectra we feel assured that the photoproduct is nitrate radical.

The measurement of NO_3 quantum yield for PAN photolysis was performed in six independent experiments. The precursor number densities ($\tilde{N}_{N_2O_5}$, $\tilde{N}_{PAN}$) and photoproduct NO_3 ratios ($[NO_3]_{PAN}/[NO_3]_{N_2O_5}$) are shown in Table 1. Taking the average of the six experiments, we find the quantum yield ($\Phi_{NO_3}^{PAN}$) to be 0.31. There are several uncertainties that need to be combined in the final reported error estimate. One error takes into account the noise (2σ) in the precursor number density, which is the largest contribution to the overall error. Another error is the noise for the photolysis product ratio involved in the relative quantum yield expression (6). These error estimates were propagated for each individual experiment to give a 2σ error estimate for each individual experiment, as listed in the right-hand column of Table 1. To combine these error estimates, we average them and find an 2σ estimate of 0.05. In addition, each of the six experiments gave a different numerical result, which we took into account by calculating the standard deviation of the individual results. This experiment-to-experiment variation gave a 2σ estimate of 0.05. We combine these two error estimates in quadrature (root-mean-square) to give an experimental precision of 0.07 (2σ). In addition to these experimental errors, we also want to consider the systematic errors. We found that the FTIR cross section error estimates were much smaller than the experimental precision, so we ignored these small errors. Because the quantum yield of the reference gas, N_2O_5 is not known at 289 nm, we consider a 10% error for this value. Addition of this 10% error in quadrature to the experimental errors gives an overall error estimate of 0.08 at the 2σ level. Therefore, our overall result is $\Phi_{NO_3}^{PAN} = 0.31 \pm 0.08$ ($\pm 2\sigma$).

Our result agrees qualitatively with previously reported results at 248 and 308 nm,[10,12] although using a different detection method for NO_3 and the wavelength is close to but not the same as the other measurements. Figure 8 plots the result of this work

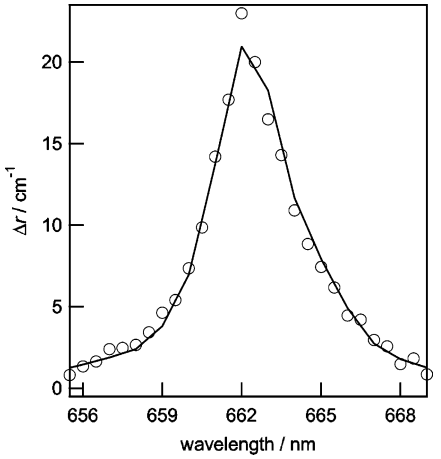

Figure 7. CRDS difference spectra recorded during PAN photolysis at 289 nm.

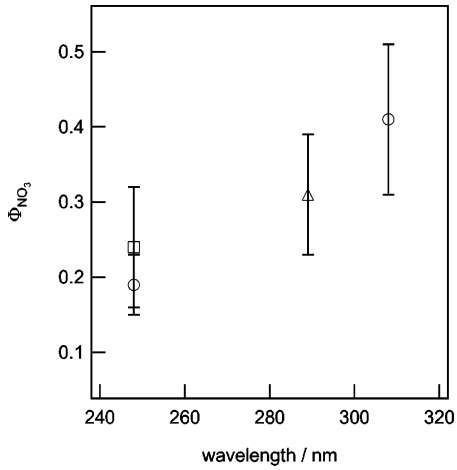

Figure 8. Nitrate radical quantum yields from PAN photolysis reported at several wavelengths. The data of Mazely et al. at 248 nm is denoted by the open box and has been adjusted as described in the text. The data of Harwood et al. at 248 and 308 nm is shown as ○. The point at 289 nm is the result of the current study and is shown as △.

along with the values reported in Harwood et al. at 248 and 308 nm and the adjusted results from Mazely et al. at 248 nm. The adjustment made to the results of Mazely et al. was to use the value for $\Phi_{NO_3}^{N_2O_5}$ of 0.80 as reported in Harwood et al.[25] The results in Figure 8 are all derived from PAN/N_2O_5photolysis experiments using different detection methods for nitrate radical. The combination of our and past work implies that as photolysis energy increases, the NO_3 quantum yield for PAN photolysis decreases, which is similar to the trend for N_2O_5. As the photolysis energy increases, more photoprocesses within NO_{3*} become possible leading to NO_3 fluorescence and direct dissociation into NO_2 and/or NO.[25,28,29] For atmospheric photochemistry, the wavelength dependence between 290 and 320 nm is of critical interest. The trend in NO_3 quantum yield for PAN is less clear in this atmospherically relevant region. Our result at 289 nm suggests a lower limit of 0.31 and an increasing trend for $\Phi_{NO_3}^{PAN}$ relevant in atmospheric chemistry models. However, there is only one measurement at 308 nm for $\Phi_{NO_3}^{PAN}$ to confirm this trend.

Conclusions

We report a photolysis quantum yield ($\Phi_{NO_3}^{PAN}$) relative to that of N_2O_5 at 289 nm of 0.31 ± 0.08 ($\pm 2\sigma$). This result is derived from six separate measurements using pump−probe CRDS experiments at the University of Alaska. Several experimental checks were performed to ensure the accuracy of the experimental results from this instrument including a detailed characterization of the performance of the ring-down cavity. These tests included establishing the proper flow conditions for the sample gases and timing of the laser shots to ensure that the photoproducts are removed from the detection volume between each laser shot. Also, a power dependence study of the reference gas N_2O_5 was performed. This check ensured that we are observing a one-photon process. Furthermore, we have investigated the temporal profiles of the cavity loss rates in the presence and absence of photoproducts to ensure there is no systematic NO_3 loss, or gain, on the time scale of the ring-down event due to flow conditions, cavity alignment, or secondary chemistry.

Figure 8 plots the results of this work along with that of the previous studies of $\Phi_{NO_3}^{PAN}$ using different experimental techniques. We find our result at 289 nm to be in qualitative agreement with the previously reported trend in results for $\Phi_{NO_3}^{PAN}$ between 248 and 308 nm. However, uncertainty in the trend at longer wavelengths indicates that consistent experiments at more wavelengths within the UV−B range would be most useful to determine whether there is a wavelength dependence for the nitrate radical quantum yield from PAN photolysis relevant to atmospheric photochemistry.

Acknowledgment. B.A.F. thanks John F. Stanton of The University of Texas for support during the initial portion of this collaboration. JFS is supported by the National Science Foundation and the Robert A. Welch Foundation. W.R.S. and M.E.A. are also supported by the National Science Foundation (CHE-0094038). We acknowledge the assistance of Sarah Kvasnicka in acquiring some of the data described in this paper. We would also like to acknowledge helpful discussions from Dr. Ruth Shear.

References and Notes

(1) Roberts, J. M. *Atmos. Environ.* **1990**, *24A*, 243.
(2) Moxim, W. J.; Levy, H., II; Kasibhatla, P. S. *J. Geophys. Res.* **1996**, *101*, 12621.
(3) Talukdar, R.; Burkholder, J.; Schmolter, A.; Roberts, J.; Wilson, R.; Ravishankara, A. *J. Geophys. Res.* **1995**, *100*, 14163.
(4) Orlando, J.; Tyndall, G.; Calvert, J. *Atmos. Environ.* **1992**, *26A*, 3111.
(5) Miller, C. E.; Lynton, J. I.; Keevil, D. M.; Francisco, J. S. *J. Phys. Chem. A.* **1999**, *103*, 11451.
(6) Bridier, I.; Caralp. F.; Loriat, H.; Lesclaux, R.; Veyret, B.; Becker, K.; Reimer, A.; Zabel, F. *J. Phys. Chem.* **1991**, *95*, 3594 and references cited within.
(7) Honrath, R. E.; Jaffe, D. A. *J. Geophys. Res.* **1992**, *97*, 20615 and Beine, H. J.; Jaffe, D. A.; Blake, D. R.; Atlas, E.; Harris, J. *J. Geophys. Res.* **1996**, *101*, 12613.
(8) Stroud, C.; Madronich, S.; Atlas, E.; Ridley, B.; Flocke, F.; Weinheimer, A.; Talbot, B.; Fried, A.; Wert, B.; Shetter, R.; Lefer, B.; Coffey, M.; Heikes, B.; Blake, D. *Atmos. Environ.* **2003**, *37*, 3351.
(9) Mazely, T.; Freidl, R.; Sander, S. *J. Phys. Chem.* **1995**, *99*, 8612.
(10) Mazely, T.; Freidl, R.; Sander, S. *J. Phys. Chem. A.* **1997**, *101*, 7090.
(11) Senum, G.; Lee, Y.; Gaffney, J. *J. Phys. Chem.* **1984**, *88*, 1269.
(12) Harwood, M.; Roberts, J.; Frost, G.; Ravishankara, A.; Burkholder, J. *J. Phys. Chem. A.* **2003**, *107*, 1148.
(13) Cavity ring-down absorption spectoscopy has been reviewed extensively in recent years and only described briefly here. The reader is directed to the review article Wheeler, M.; Neuman, S.; Orr-Ewing, A.; Ashfold, M. *J. Chem. Soc., Faraday Trans.* **1998**, *94*, 337 for further detail.
(14) Chen, Y.; Zhu, L. *J. Phys. Chem. A.* **2003**, *107*, 4643 and references cited within.
(15) Brown, S.; Ravishankara, A. R.; Stark, H. *J. Phys. Chem. A.* **2000**, *104*, 7044.
(16) Tsalkani, N.; Toupance, G. *Atmos. Environ.* **1989**, *23*, 1849.
(17) Gaffney, J.; Fajer, R.; Senum, G. *Atmos. Environ.* **1984**, *18*, 215.
(18) Angerhofer, M. Photodissociation and Quantum Yield Determination of Peroxyacetyl Nitrate. M.S. Thesis, University of Alaska, Fairbanks, AK, 2003.
(19) Wanberg, I.; Etzkorn, T.; Barnes, I.; Platt, U.; Becker, K. *J. Phys. Chem. A.* **1997**, *101*, 9694.
(20) Cooper, J.; Zare, R. *J. Chem. Phys.* **1968**, *48*, 942.
(21) Wayne, R.; Barnes, I.; Biggs, P.; Burrows, J.; Canosa-Mas, C.; Hjorth, J.; Le Bras, G.; Moortgat, G.; Perner, D.; Poulet, G.; Restelli, G.; Sidebottom, H. *Atmos. Environ.* **1991**, *25A* (1), 1.
(22) King, M.; Dick, E.; Simpson, W. *Atmos. Environ.* **2000**, *34*, 685.
(23) Davidson, D.; Viggiano, A.; Howard, C.; Dotan, L.; Fehsenfeld, F.; Albritton, D.; Ferguson, E. *J. Chem. Phys.* **1978**, *68*, 2085.
(24) Wanberg, I.; Etzkorn, T.; Barnes, I., Platt, U.; and Becker, K.; *J. Phys. Chem. A.*, 101, 9694.
(25) Cantrell, C.; Davidson, J.; McDaniel, A.; Shetter, R.; Calvert, J. *J. Chem. Phys.* **1988**, *88*, 4997.
(26) Harwood, M.; Burkholder, J.; Ravishankara, A. *J. Phys. Chem. A.* **1998**, *102*, 1309 and references cited within.
(27) Sander, S. P.; Freidl, R. R.; Golden, D. M.; Kurylo, M. J.; Huie, R. E.; Orkin, V. L.; Moortgat, G. K.; Ravishankara, A. R.; Kolb, C. E.; Molina, M. J.; Finlayson-Pitts, B. J. *Chemical Kinetics and Photochemical Data for Use in Atmospheric Studies*; Evaluation 14, Publication 02-25; NASA/Jet Propulsion Laboratory: Pasadena, CA, 2003, and references cited within.
(28) Torabi, A. An Investigation of the Kinetics and Excited-State Dynamics of the Nitrate Free Radical. Ph.D. Thesis, Georgia Institute of Technology 1985.
(29) Oh, D.; Sisk, W.; Young, A.; Johnston, H. S. *J. Chem. Phys.* **1986**, *85*, 154.
(30) Johnston, H. S.; Davis, H. F.; Lee, Y. T. *J. Phys. Chem.* **1996**, *100*, 4713.